Colloids and Surfaces A: Physicochemical and Engineering Aspects 653 (2022) 129833

Contents lists available at ScienceDirect

Colloids and Surfaces A: Physicochemical and Engineering Aspects

journal homepage: www.elsevier.com/locate/colsurfa

An accelerated antibody aggregation test based on time sequenced dynamic light scattering

Cathryn G. Conner [a], James McAndrew [b], Stefano Menegatti [a], Orlin D. Velev [a,*]

[a] Department of Chemical and Biomolecular Engineering, North Carolina State University, Raleigh, NC 27695, USA
[b] Air Liquide, 200 GBC Ave, Newark, DE 19702, USA

HIGHLIGHTS

- Size distribution data from light scattering are sensitive indicators of protein aggregation.
- Elevated temperatures enable accelerated evaluation of antibody colloidal stability.
- Temporal evolution of size distributions conveniently reveals onset and rate of aggregation.
- Aggregation rates depend strongly on antibody concentration and buffer conditions.
- The presence of pre-existing (seed) protein aggregates accelerates aggregation rate.

GRAPHICAL ABSTRACT

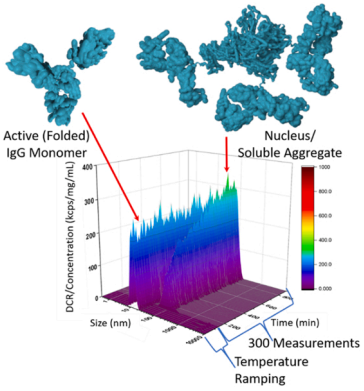

ARTICLE INFO

Keywords:
Protein colloidal stability
Protein aggregation
Dynamic light scattering
Antibodies

ABSTRACT

A rapid method for determination of the colloidal stability of protein molecules in solution is reported as an efficient tool for evaluating the stability of antibody formulations. Using human polyclonal immunoglobulin G (IgG) as a model protein and dynamic light scattering (DLS) as a technique to determine the size of particles in solution, the rate of aggregation is investigated at different temperatures and antibody concentrations. To reduce the observation period while increasing precision, a new approach to DLS analysis is developed that comprises: (*i*) a distribution analysis of high-resolution data, and fitting for multiple particle sizes present in a solution, (*ii*) a temperature ramp to an intermediate temperature followed by a stress test at constant temperature over several hours, and (*iii*) 3-D plotting to reveal the time-dependent evolution of the particle size distribution at the selected temperature. The resulting 3-D plots enable robust identification of the onset of aggregation with different dispersion conditions. This method enables rapid evaluation of the effects of parameters such as temperature and concentration on the stability of antibody solutions.

* Corresponding author.
E-mail address: odvelev@ncsu.edu (O.D. Velev).

https://doi.org/10.1016/j.colsurfa.2022.129833
Received 7 June 2022; Received in revised form 27 July 2022; Accepted 28 July 2022
Available online 4 August 2022

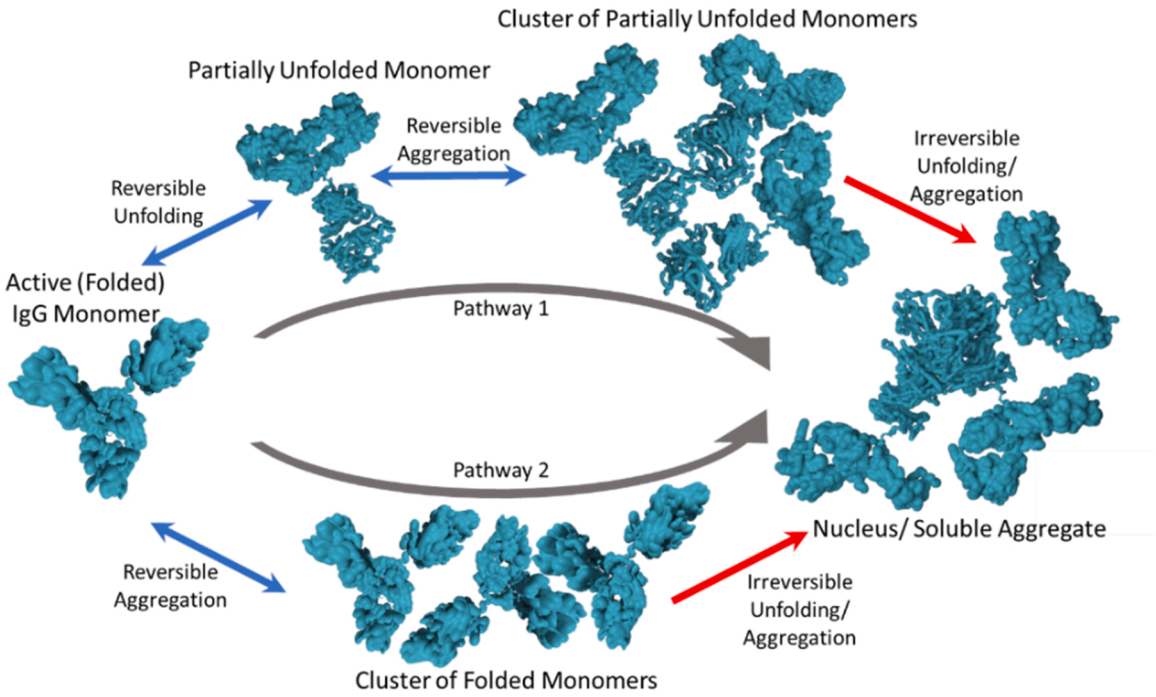

Fig. 1. Schematic of the two major pathways leading to irreversible IgG aggregation. In the first pathway, the native folded monomers (models from the protein data bank) [17] first become partially unfolded. These partially unfolded monomers reversibly cluster together and subsequently aggregate irreversibly. In the second pathway for IgG aggregation, active monomers reversibly form a cluster together. This is followed by irreversible agglomeration.

1. Introduction

The past two decades have seen the rapid expansion of monoclonal antibody-based therapies in the treatment of cancer, autoimmune and degenerative diseases [1–3]. While well-known for their biochemical stability, antibodies are, similarly to all proteins, prone to denaturation and aggregation [2,4,5]. Their aggregates in particular pose a serious safety threat to patients, due to their documented immunogenicity [6–8]. Accordingly, improvements in formulations, storage conditions and the product purity that prolong the long-term colloidal stability of therapeutic antibody solutions are urgently needed in order to prevent health risks and minimize economic losses that pharmaceutical companies and healthcare systems incur.

The majority of therapeutic antibodies currently on the market belong to the Immunoglobulin G (IgG) family, and in particular to IgG_1 and IgG_4 subclasses, [9] while a smaller portion belong to IgA and IgM families [10]. IgGs consist of four polypeptide chains – specifically, two heavy chains and two light chains – joined by disulfide bonds and arranged into a Y-shaped structure comprising a constant Fc (fragment crystallizable) region and two variable Fab (fragment antigen binding) segments [11,12]. Prior research has identified two likely pathways to the irreversible formation of aggregates from systems of IgG monomers. These pathways are illustrated in Fig. 1. The first pathway includes three main steps, the first of which is the reversible partial unfolding of a monomer. Notably, Fig. 1 illustrates the unfolding of the Fc region, which is more prone to initiate the aggregation process [13]. The second step is reversible clustering of the partially unfolded monomers. The third, and final, step along this pathway is the irreversible agglomeration of the clustered and partially unfolded monomers. The second pathway to the formation of soluble aggregates from protein monomers includes only two steps: the reversible clustering of folded monomers followed by irreversible agglomeration [14–16].

Many studies have been focused on predicting the factors impacting the long-term stability of IgG monomers with short term tests and simulations [9,18–25]. Experimental methods to detect and quantify protein aggregation include mass spectrometry, size exclusion chromatography (SEC), field-flow fractionation (FFF), and analytical ultracentrifugation (AUC). These methods are useful in that they can determine the mass fraction of unaggregated protein, output size distributions, and account for insoluble aggregates [26–28]. However, these techniques physically stress the sample, so they have the potential to either disrupt existing aggregates or form new aggregates during the analysis of the samples [24]. In addition, they are not sufficiently sensitive to detect the onset of aggregation at very low concentrations. Conversely, light scattering techniques do not account for insoluble protein or provide mass fraction data, but they also do not physically stress the samples or cause aggregation during data collection [24, 29–32]. Light scattering methods are exquisitely sensitive to extremely low amounts of moderate-size particles (due to the variation of light scattering with the 6th power of the particle size). Thus, they can detect aggregation levels far below the detection limit of the techniques mentioned above.

One light scattering technique used for determining stability of colloids is electrophoretic light scattering (ELS), which outputs electrophoretic mobility and ζ-potential values related to surface charge. However, the ionic strengths of physiological buffers for IgG pharmaceutical formulations are usually too high for reliable ζ-potential measurements. Adopting a conventional buffer would make it more challenging to identify reliable correlations for the long-term stability of proteins in their native buffered solutions [33]. Additionally, IgG solutions in pharmaceutical applications are frequently buffered to a pH where the proteins may be relatively weakly charged, making it difficult to accurately obtain their ζ-potential [34,35].

Another common method used to analyze colloidal dispersions is dynamic light scattering (DLS). DLS is typically used to determine the average size of approximately spherical particles in stable, dilute dispersions, and its basic output is the average hydrodynamic diameter [36–39]. For IgG, the hydrodynamic diameter is close to the largest dimension of the protein, about 11 nm for a monomer [40]. A larger average size reported by DLS indicates the presence of aggregates, with extreme sensitivity, as mentioned above, as even a single aggregate within the miniscule volume of the laser focus can strongly affect the

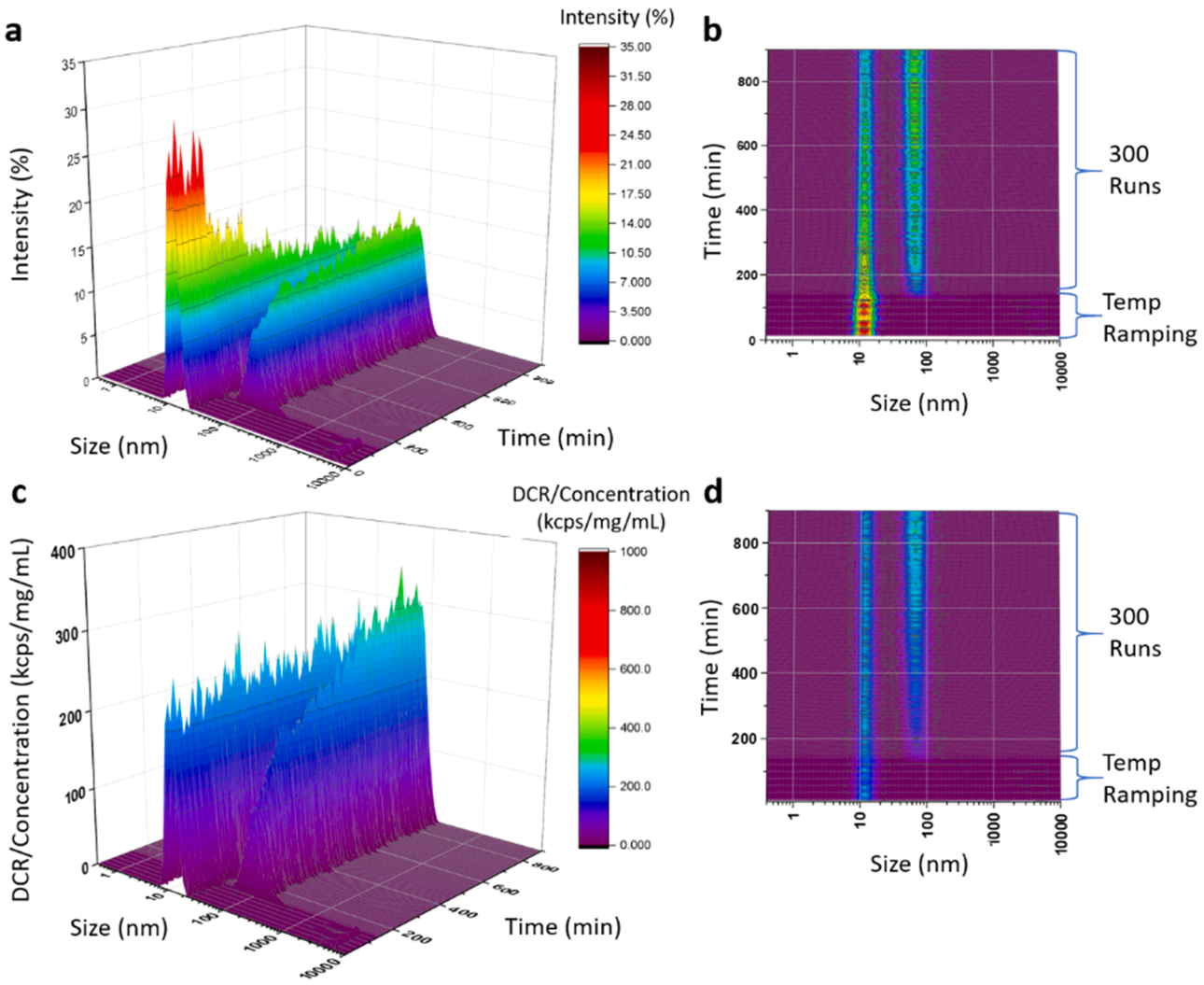

Fig. 2. 3-D plots of 2.5 mg mL^{-1} IgG in 0.15 M PBS demonstrating aggregation via size distributions over time for a period of temperature ramping, up to 55 °C, followed by consecutive measurements at 55 °C. The results are plotted (a) with intensity on the z-axis from the side and (b) as color coded map from above. Intensity distributions in (a) and (b) are expressed in terms of normalized intensity values. This makes comparison across samples difficult. These results are re-plotted in (c) and (d) with derived count rate (DCR) divided by IgG concentration. By switching from intensity to DCR/concentration, plots of different sample concentrations can be easily compared.

reported size [41–43]. DLS has also been applied to the detailed investigation of aggregate size of polymers [44,45]. In the case of IgG, however, precise quantification of aggregate size is much more challenging. Nevertheless, it is generally accepted that DLS is a useful indicator of IgG aggregation [46] and we aim to further extend its efficiency and capabilities here.

One approach for rapid testing of the stability of different protein dispersions was developed using Malvern DLS instrumentation. The system utilized in the technique combines DLS and Raman Spectroscopy with a programmable temperature ramping platform, allowing the sample to thermally equilibrate before acquiring data at a given temperature and proceeding with the temperature ramp [47,48]. At each temperature, the average particle size is calculated, and the protein conformation is determined. This analysis can be completed in a few hours and, on the DLS side, highlights differences in stability for protein dispersions that have different aggregation points. The aggregation point coincides with the temperature at which the average protein cluster size begins to increase rapidly [49]. While dispersions with different buffer additives may have different aggregation points visible with the described technique, small changes in concentration and storage temperature cannot be analyzed.

In this study, we report the development of a rapid and facile DLS-based colloidal stability assay featuring a novel approach to process and present the data more accurately, and predict the long-term stability of protein solutions. We demonstrate how this stability assay can be used to evaluate the aggregation rate of solutions of human polyclonal IgG antibodies in physiological buffer as a function of the IgG concentration and temperature. In addition, the impact on stability of preexisting aggregates in the dispersion of IgG protein was investigated.

2. Results and discussion

The DLS-based technique for determining long term protein colloidal stability is based on a modified Malvern instrumentation routine. The key result obtained from the original implementation of the method is the temperature at the point of aggregation [49]. However, the method's algorithm continues to ramp the sample temperature beyond that point, collecting rapidly increasing average aggregation data illustrated in Fig. S1. This poses two main issues: first, the aggregation rate rapidly accelerates as the temperature increases, which complicates accurate determination of the aggregation onset. Second, the simple cumulant fit utilized by the software cannot capture the main characteristics of

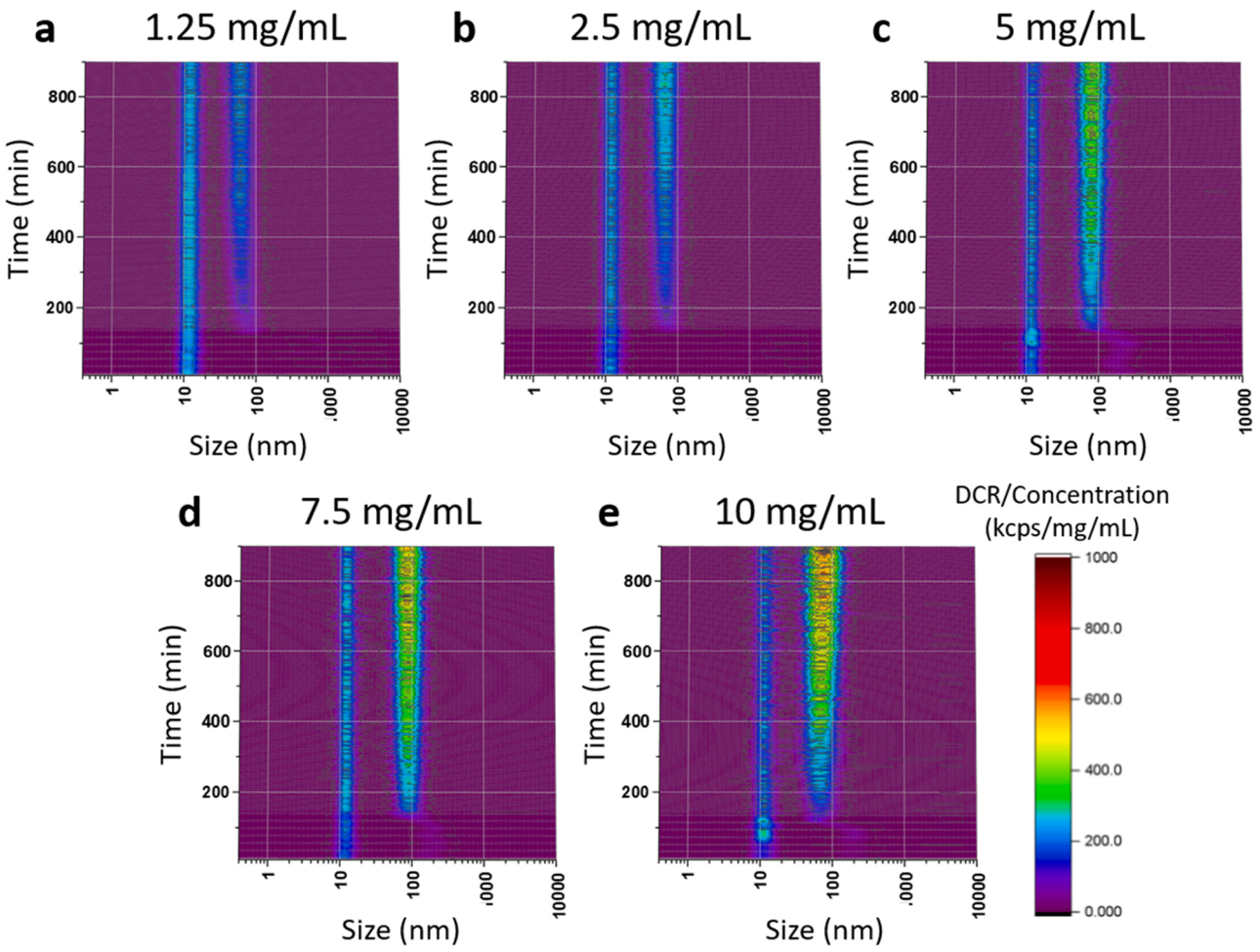

Fig. 3. 3-D plots of DCR/concentration (as defined in the text) showing the rate of IgG aggregation in 0.15 PBS, visualized by the rate at which the aggregate size distribution peak (to the right of each graph) evolves, with respect to the original IgG monomer concentration (left peak). Data plotted for concentrations of (a) 1.25 mg mL^{-1}, (b) 2.5 mg mL^{-1}, (c) 5 mg mL^{-1}, (d) 7.5 mg mL^{-1}, and (e) 10 mg mL^{-1}. Each plot contains a ramping section from 25 °C to 55 °C, followed by consecutive measurements at 55 °C. As expected, the aggregation is more pronounced at higher protein concentrations.

particle size distributions as aggregation proceeds. The cumulant fit outputs a single size average and polydispersity [50,51]. In reality, the size of the protein is not growing exponentially, but aggregates are contributing to a multimodal size distribution that the cumulant fit cannot approximate adequately.

In our approach, a multicomponent distribution fit is employed in lieu of the cumulant fit [52,53]. This option is offered by most modern DLS instruments, including the Malvern Instruments Zetasizer used in this study. While the multicomponent distribution fit is more flexible than the cumulant fit, its limitations must also be considered. The main concern is that it may not capture every particle size present in the system. All DLS approaches rely on measuring and fitting the exponential correlation decay of the sample light scattering. Most fitting algorithms minimize the number of parameters used to fit the decay, and therefore they may not report accurately all different particle sizes present in solution. The absence of a particle size in the fitted distribution does not imply that particles of that size are not present in the real sample, only that the measured decay can be fit without them. Despite this limitation, the multicomponent distribution fit identifies and displays the presence of aggregate particles far more effectively than the cumulant fit, as demonstrated by our results. Our method for probing the stability of proteins combines this highly sensitive data fitting routine with more meticulous identification and analysis of the aggregation point.

2.1. Generating 3-D plots to analyze protein aggregation

Our method ramps the sample temperature up to the aggregation point, then sustains the sample at that temperature while collecting DLS data approximately every 3 mins for 300 measurements. The higher temperature, determined by preliminary sample measurements that implemented temperature ramps, accelerates the aggregation rate of the antibodies in sample, enabling rapid evaluation of the protein stability in the selected medium. Elevating the sample temperature has been used in literature to predict the stability of protein dispersions, but those methods did not make use of continuous measurements for accuracy and detail in short time periods [25,54–59]. The time required for each size measurement is dispersion-dependent, since the Malvern software automatically increases the measurement time for larger and more polydisperse samples. For a stable sample of smaller size populations, such as proteins, the average instrument measurement time is 3 mins. Thus, we elected to perform 300 measurements at the final ramping temperature, for a full experiment time of ~15 h, resulting in a large amount of data over reasonably long experimental duration.

When all size distributions from temperature ramping and consecutive measurements at the final elevated temperature are collectively plotted, 3-D plots with surface contour mapping are generated as illustrated by the data plotted in Fig. 2. The default size distribution for the Zetasizer software is based on intensity % values, as in Fig. 2a and b. Of the three distributions generated by the software – namely, intensity,

volume, and number – intensity is closest to the raw data as it refers to the photons scattered by particles of different sizes. In addition, all aggregates appear on the distribution, enabling the monitoring of the aggregation process from its very onset. Using intensity-based plots provides insight on the rate of aggregation before the aggregates can be registered by other methods such as size exclusion chromatography (SEC).

The main challenge in comparing consecutive intensity-based size distributions, generated by the Zetasizer software, is that they do not take into account that the total scattered light intensity changes dramatically during the experiment, due to the increasing number of aggregate particles. Accordingly, the monomer peak (on the left) of Fig. 2a and its projection in Fig. 2b decrease rapidly, even though the absolute population of monomers is hardly changing. To analyze multiple related measurements, as the 3-D plots, a plot taking absolute intensity changes into account was constructed using the Derived Count Rate (DCR) associated with each measurement. [52] DCR values are calculated from the count rate (measured light intensity) during a measurement and the attenuator setting, as shown in Eq. (1). The attenuator blocks a portion of the sample's scattered light so that the photon detector conducts the counting in its ideal range. Therefore, DCR represents the count rate if there was no attenuator in use and has units of kilo-counts per second (kcps).

$$\text{DCR} \sim \text{Count Rate} \bullet \text{Attenuator Factor} \quad (1)$$

Eq. (1) gives the total DCR for a given measurement, which can be generalized to DCR as a function of apparent particle size, which we denote DCR(*size*) by taking the product of DCR with the Intensity % size distribution returned by the instrument, as in Eq. (2):

$$DCR(size) = DCR \bullet \text{Intensity } \%\ (size) \quad (2)$$

We note that "Intensity % (*size*)" is proportional to the relaxation time distribution spectrum obtained from the intensity auto-correlation function, where the relaxation times are assumed dependent on the hydrodynamic radius. Since the instrument does not provide direct measurement of the absolute light intensity associated with a given particle size, we calculated it using Eq. (2).

As a further normalization, by dividing the DCR by the IgG concentration in the sample, aggregation rates of different concentrations can also be compared due to similar scattering intensities at the start of measurements. This fully developed 3-D plot, the data presentation format for the remainder of this paper, using DCR/Concentration for the z-axis units is shown in Fig. 2c, and projected in color code in Fig. 2d. The two plots show that the light scattering due to the monomer population hardly evolves over the course of the experiment, while the scattering due to the aggregate peak increases; furthermore, a small population of aggregates results in a strong light scattering signal due to the particle size-dependence of the scattered light intensity.

In reviewing plots such as those shown in Fig. 2, it is tempting to conclude that the particle size distribution is strictly bimodal, and aggregates form with a narrow size distribution (about 80 nm). That interpretation is not justified, as discussed earlier. The presence of a single aggregate peak merely indicates that a good fit to the time-dependent correlogram can be obtained by assuming a narrow aggregate size distribution. Aggregates of intermediate size may also be present, but their effect on the relaxation time spectrum is not resolvable. In subsequent discussions, we will assume that the intensity of the aggregate peak is proportional to the aggregate concentration and that its rate of change can be used as a measure of the rate of the aggregation reaction. We find that this assumption gives reasonable results as in our experiments, where the amount of aggregates remains small and the aggregate size distribution does not appear to undergo any dramatic changes.

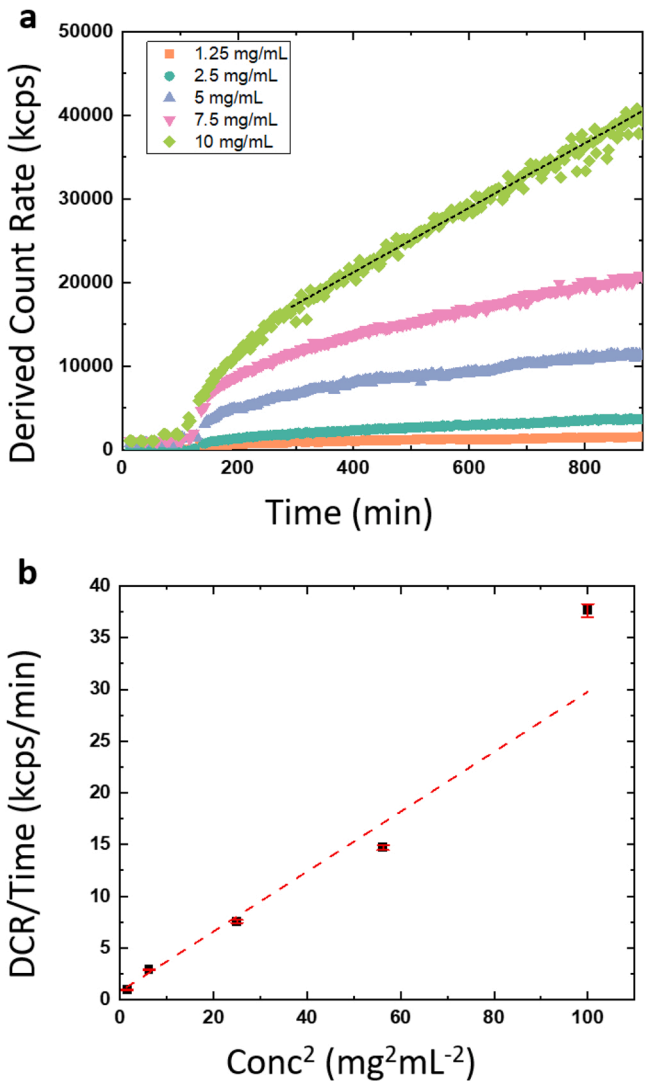

Fig. 4. Plots for analysis of aggregation rate at different IgG concentrations, showing (a) the raw data of derived count rate under the aggregate peak over time for each concentration. (b) The slopes from the raw data are plotted versus concentration squared after fitting the linear region for each curve, from 300 mins to 900 mins. The linear least-squares fit line indicates that the aggregation of protein is a second order process ($R^2 = 0.97$).

2.2. Correlating aggregation rate and sample concentration

By plotting the time-dependent DLS data (i.e. DCR/concentration vs particle size over time) for different IgG concentrations in solution, the method allows to clearly present and compare the difference in aggregation rate, and therefore dispersion stability, as shown in Fig. 3. At each concentration tested, ranging from 1.25 mg mL^{-1} to 10 mg mL^{-1} (Fig. 3a–e), the position of the first peak, i.e., the monomer peak, remains constant throughout the measurements. Meanwhile, the second peak, which is indicative of aggregates, becomes more pronounced in each plot with increasing concentration.

In keeping with the goal of predicting the long-term stability of a protein in solution, the visual information provided by 3-D plots as a final output overcomplicates the analysis in some cases. In order to extract predictive descriptors from the 3-D plots, the area under the curve for the second peak in the DCR plot (without concentration normalization) was extracted for each measurement and plotted vs. measurement time as shown in Fig. 4a. Since this peak is produced by the aggregates formed at different IgG titers in solution, the rate at

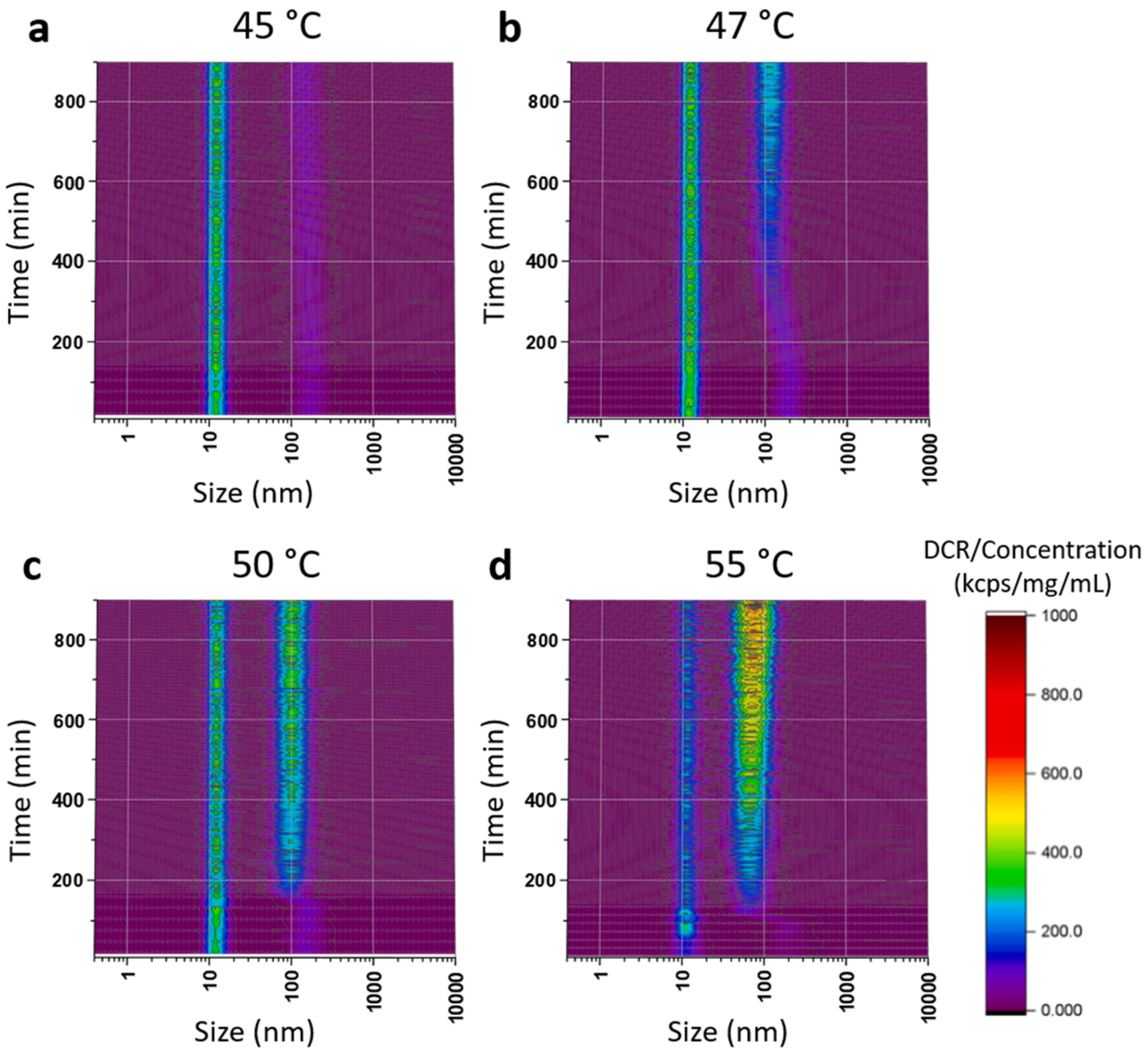

Fig. 5. 3-D plots showing how the aggregation rate of 10 mg mL^{-1} IgG in 0.15 M PBS increases as the final ramping temperature and consecutive measurements' temperature is set to (a) 45 °C, (b) 47 °C, (c) 50 °C, and (d) 55 °C.

which the area under the aggregate curve increases can be correlated to the aggregation rate at the elevated temperature, as shown in Eq. (3).

$$\frac{Total\ \ DCR\ \ of\ \ 2nd\ \ peak}{Time} \sim \frac{Extent\ \ of\ \ aggregation}{Time} \quad (3)$$

This aggregation rate at higher temperature can ultimately be correlated to the aggregation rate at room temperature according to prior research [25].

All IgG samples begin to register aggregation after the temperature ramp reaches 55 °C at approximately 140 mins, corresponding to the peak onset seen in Fig. 4a (a slight initial increase peak area during the ramp is visible at 10 mg mL^{-1}). The subsequent increase in observed peak area at a steady temperature of 55 °C can be described by two regimes. First, we see a period of accelerated aggregation where the intensity increases rapidly within an intermittent period of ≈ 160 mins. At times larger than 300 mins, all intensity profiles follow an approximately linear increase over time, suggesting a steady-state aggregation process. Thus, we performed an analysis of the linear regimes of the data from 300 to 900 mins for each curve (Table S1). The slope of the fitted line in this interval is proportional to the aggregation rate (Eq. (3)) and allows to evaluate the kinetics of the process.

The process of self-aggregation of a single species is commonly described by a second-order kinetics model, $r = k[A]^2$, where r is the reaction rate and $[A]$ is the concentration of the reacting species. The classic approach to demonstrating second order kinetics is a plot of the reciprocal of the reactant concentration vs. time. That approach is not satisfactory here, because the change in concentration of the IgG monomer is barely detectable. However, the rate of formation of aggregates is easily quantified by our method, and reaction order can be assessed by the method illustrated in Fig. 4b. This plot shows a relatively good correspondence to the second order kinetics model ($R^2 = 0.97$), while other ways of plotting these data such as $r = k[A]$, had much worse fit ($R^2 = 0.87$). Overall, Figs. 3 and 4, and especially Fig. 4b, provide evidence that the antibody aggregation rate in the longer term has a second order dependence on IgG concentration, as commonly expected based on established literature [60–62].

2.3. Correlating aggregation rate and temperature

Another effect that is likely correlated to the long-term stability of

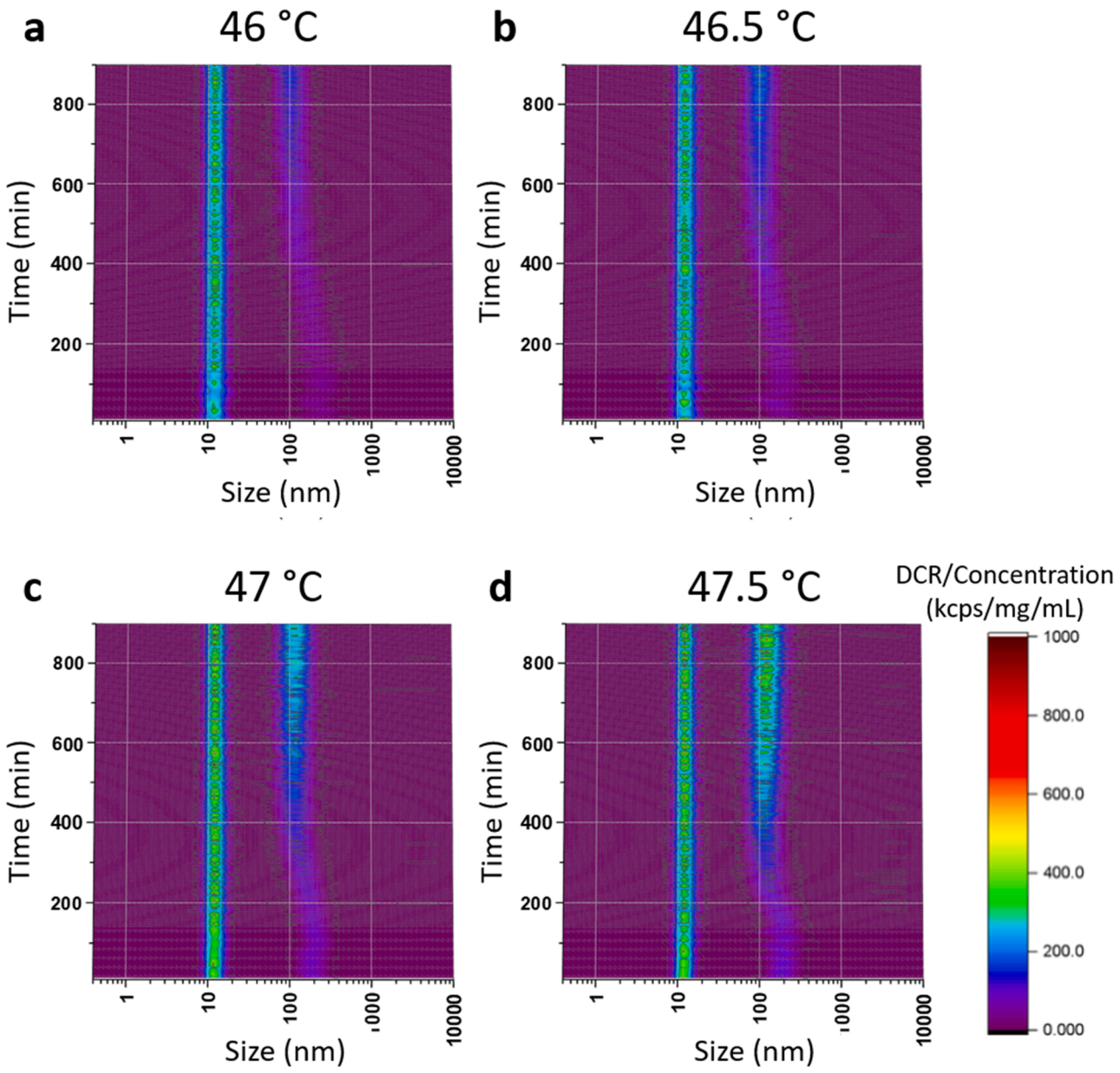

Fig. 6. 3-D plots showing increasing intensity of aggregate peaks with increases in final temperature for 10 mg mL^{-1} IgG in 0.15 M PBS. The samples were ramped up to (a) 46 °C, (b) 46.5 °C, (c) 47 °C, and (d) 47.5 °C. The data show that even an increase of half a degree in the final ramping temperature results in a visibly more intense plots and therefore faster aggregation.

protein samples is the impact of temperature on the aggregation rate. Previous research by other techniques has concluded that protein aggregation rate at an elevated temperature can be correlated with the rate of aggregation at room temperature [25]. Our method includes a temperature ramping section, which can be stopped at varying temperatures enabling the observation of the onset and evolution of antibody aggregation in real time using subsequent consecutive light scattering measurements. Fig. 5 illustrates how the rate of aggregation of samples of 10 mg mL^{-1} IgG markedly changes as the final temperature is varied between 45 °C and 55 °C with intervals of 2–5 °C.

The intensity of the aggregate peak increased significantly within the interval of temperatures plotted in Fig. 5. Therefore, we investigated how even smaller changes in the ramping temperature can result in 3-D plots revealing different rates of aggregation, as shown in Fig. 6, which reports the experiments with final temperatures from 46 °C to 47.5 °C, increasing in intervals of 0.5 °C. While these changes in final temperature are small, the change in aggregation rate is apparent, demonstrating the sensitivity of the method and the existence of a point of thermal threshold of rapid aggregation.

As before, the data shown in the 3-D plots of Figs. 5 and 6 can be studied and interpreted conveniently by focusing on the area under the second size distribution peak. These data are plotted in Fig. 7. The two regimes, rapid initial growth, and steady linear increase, observed at 55 °C (see discussion of Fig. 4) are still visible at 50 °C, but are not present at lower temperatures. This suggests that we are observing one process that is activated at ~ 45 °C, followed up with another one beginning around 50 °C. For the concentration-dependent data discussed earlier, which were collected at 55 °C, the first process accounts for the initial rapid increase in peak area while the second was shown to have second order kinetics. Re-examining Fig. 7 in detail shows that there is a change in the rate-determining process at ≈ 50 °C, where we observe a rapid increase in aggregate concentration followed by almost no growth, and then the emergence of a new rate-determining step by 55 °C.

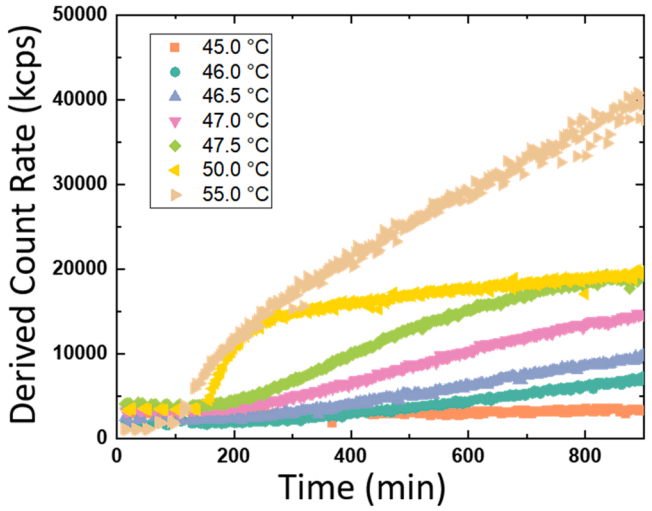

Fig. 7. Impact of final elevated temperature on the aggregation rate of 10 mg mL^{-1} IgG dispersions. The total area under the aggregate size distribution peaks in the previous two figures are extracted to plot (a) the derived count rate over time for aggregates present in suspension. Except for the experiment ramped to and held at 50 °C, there is a visibly steady increase in the aggregation rate as the final temperature is increased.

Although the elucidation of the detailed mechanism of protein aggregation is beyond the goals and means of this study, we can hypothesize to what extent our data are consistent with the generally accepted mechanisms illustrated in Fig. 1. We performed a basic analysis of the activation energy of the aggregation processes, based on the classical Arrhenius equation. These results, described in Fig. S2 and Fig. S3 in the Supplemental Information, suggest that below 50 °C the rate determining step has a high activation energy (~ 290 kcal mol^{-1} – see the Supplementary Information for a discussion of the evaluation and uncertainty in this value), which decreases significantly at higher temperatures (~ 60 kcal mol^{-1}). Based on these estimates, as well as the information in Figs. 4 and 7, we propose at $T > 50$ °C a mechanism involving two processes, one of which shows an activation energy in the range corresponding to unfolding, and the other following second order kinetics and therefore postulated to be aggregation. A change from first order to second order kinetics can explain the emergence of a lower activation energy at higher temperature, which is difficult to account for otherwise. While we attribute the process responsible of the initial rapid rise in signal to unfolding (first order kinetics process), this does not necessarily mean that unfolding occurs first at the molecular level, but rather that unfolding is the rate determining step at early times, while later on aggregation becomes rate determining. This might occur if (for example) there is a transient population of "reversible" aggregates present at ambient temperature, that unfold rapidly once the temperature becomes high enough, consistent with the pathways outlined in Fig. 1.

2.4. Impact of preexisting aggregates on aggregation rate

A common theory in the literature on protein aggregation is that the first aggregates formed in the protein solution act as seeds or catalysts, promoting further aggregation. This suggests that, barring the differences observed among the aggregation rates in the solutions at different protein concentrations, solutions with equal concentration may experience different rates of aggregation should they contain different fractions of aggregate seeds, while maintaining all other parameters constant. To evaluate this, selected IgG solutions were processed through a filter with 20 nm pores (in lieu of the 200 nm pores used before) prior to DLS investigation in the Zetasizer. The results are shown in Fig. 8.

Upon subjecting the samples to filtration using a much lower cutoff filter, substantially lower aggregation was observed, partially due to a delayed onset of aggregation. As described in the previous section, the final temperature set (55 °C) accelerates aggregation and delivers detailed data very rapidly. However, the onset of aggregation was observed much later in the 20 nm-filtered samples where the initial aggregates were removed.

As the plots in Fig. 8 show a lower aggregation rate for samples without initial "seed" aggregates, we inquired whether using 20 nm pore filters reduced the IgG concentration in solution compared to the samples treated with 200 nm pore filters. Different protein concentrations result in a definite change in the aggregation rate. Table S2 reports the values of concentration measured in the IgG solutions before and after filtration through either 200 nm or 20 nm pores. As anticipated, the loss in IgG titer upon filtration is negligible, since the number of native aggregates is small. These data conclusively confirm that the presence of seed aggregates is a key factor accelerating protein aggregation in solution during storage.

Our observations in this section are generally consistent with the mechanism discussed in the previous section, where a rapid unfolding process, governed by initial aggregate levels, is rate-determining at early times, but eventually gives way to a rate-determining aggregation process as initial aggregate levels are depleted.

3. Concluding remarks and outlook

We present a method enabling the rapid and highly sensitive analysis of the stability of protein solutions based on dynamic light scattering data. The method employs a programmed temperature ramp to bring the protein sample to a temperature at which aggregation can be followed in real time. Once this threshold point is reached, the sample is maintained at that temperature while consecutive size measurements are collected. The method was augmented by designing new protocols of data collection and analysis. Instead of calculating and reporting solely the average size, the entire size distributions were processed, and plotted over time in a 3-D plot. The size distributions can be either plotted as intensity percent or, to make plots better reflect changes in the concentration of monomers and aggregates, they were changed to derived count rate. The 3-D plotting of the time-dependent size distribution allows clear visualization of the moment of IgG aggregation and the kinetics of the process, as the aggregate peak grows over time. The 3-D color mapping also provides a means to accurately identify the moment of aggregation and comparing the stability of IgG samples of varying concentrations or under different solution conditions.

The proposed method is quite convenient and informative for understanding aggregation of antibodies and other protein formulations in solution. For example, we were able to demonstrate the effect of trace levels of aggregates on the subsequent aggregation rate. Although this result was expected, we did not find any other study in which it was clearly observed. Similarly, we expect that various improvements, for example, improved formulations in solution, can be rapidly evaluated by our method prior to being rigorously tested by more exhaustive approaches. While we have developed our method using polyclonal antibodies, there is no reason (other than the cost of the materials being tested) why it cannot be applied to monoclonal antibodies and realistic therapeutic formulations. Furthermore, accelerated testing of IgG stability against aggregation can support the biomanufacturing processes of IgG at different stages, such as evaluating the clarified cell culture harvests, the effluent of low-pH viral inactivation phase, and the concentrated and conditioned products of ultrafiltration. In light of the unique importance of antibodies in modern medicine and biotechnology, we focused exclusively on IgG in this study. One can reasonably expect that the same methodology is widely applicable to other protein solutions with minor adjustments, although it was not practical to test that in this study nor was it obvious which other proteins should be adopted.

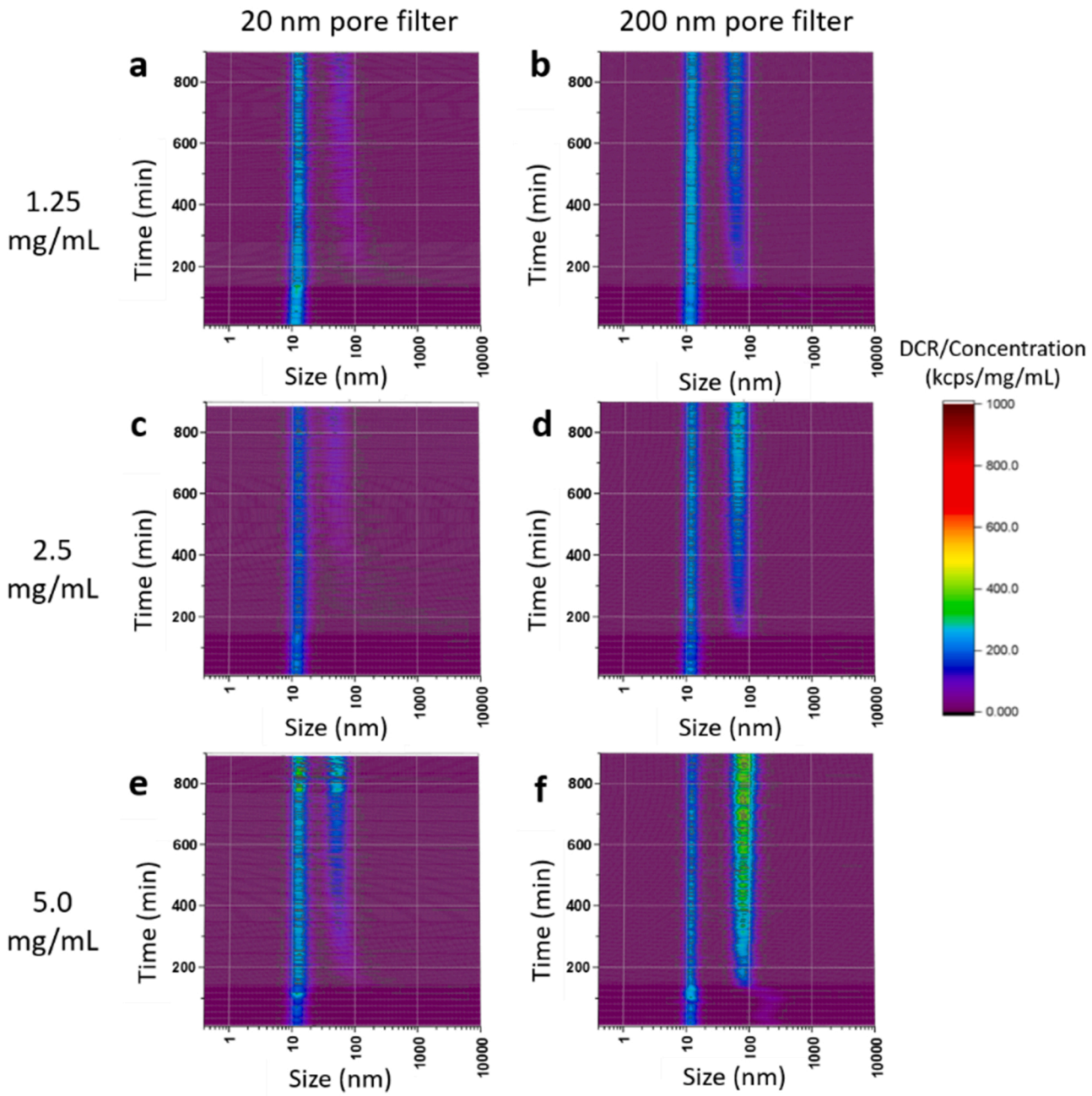

Fig. 8. 3-D plots showing the difference in the rate of aggregation of IgG solutions of different concentration before and after filtration with a fine 20 nm pore cut-off filter. Each plot of IgG solution in 0.15 M PBS contains a ramping section from 25 °C to 55 °C followed by consecutive measurements at 55 °C. The data for samples that were filtered with 20 nm pores are shown in plots (a) 1.25 mg mL^{-1}, (c) 2.5 mg mL^{-1}, and (e) 5 mg mL^{-1}. They are compared with the (previously shown) data for samples at the same concentration filtered with 200 nm pores in (b), (d) and (f). The results demonstrate that the finely filtered samples begin to aggregate much later and at a slower rate.

Further improvements to the method reported here can be achieved by optimizing instrument capabilities or operating parameters. The use of a multi-angle light scattering method might allow more detailed interpretation of the measured particle size distribution. In applications where the accuracy of measuring the parameters for the monomer peak is not important, forward-angle scattered light can provide increased sensitivity to the detection of small aggregates. Finally, similar methods can be applied for identification of the factors leading to aggregation in biomanufacturing and initial optimization of additives and other approaches to their inhibition. We expect that additional applications will naturally arise if this approach is used more widely, due to its combination of convenience with extreme sensitivity to the onset of aggregation.

4. Experimental section

Materials: Lyophilized polyclonal Immunoglobulin G (IgG) from normal human plasma (Lot# 2017–01) was purchased from Athens Research and Technology. Deionized water, used for the reconstitution of protein, was obtained from a Millipore RiOS system equipped with a Synergy UV module. Phosphate buffered saline (PBS) tablets, used to make 0.15 M PBS, were purchased from Sigma-Aldrich Inc. Two types of syringe filters, Millex-GV Filters with a diameter of 13 mm and pores that are 0.22 μm and Whatman Anotop 10 filters with a diameter of 10 mm and pores that are 0.02 μm, were purchased from Millipore-Sigma. 2 mL clear glass threaded vials with closures and 1 mL BD sterile syringes with slip tips were purchased from Fisher Scientific.

Preparation of IgG samples: IgG is first reconstituted to its original concentration. The dry product received from Athens Research and Technology had an original volume of 25.1 mL and original concentration of 41.8 mg·mL^{-1} IgG. After lyophilization, the mass of the product was 1352 mg according to the company. The original mass and volume were used to calculate the desired mass and volume of DI water required for a set of experiments as the entire bottle was not reconstituted at once. After reconstitution to 41.6 mg mL^{-1}, the dispersion was diluted down to the desired working concentrations (1.25 mg mL^{-1}, 2.5 mg mL^{-1}, 5 mg mL^{-1}, 7.5 mg mL^{-1}, and 10 mg mL^{-1}) using 0.15 M PBS. The final samples were filtered into 2 mL glass vials for storage and measurement.

Analysis with Dynamic Light Scattering: Size distributions, indicative of monomers and aggregates present in dispersion, were measured through dynamic light scattering using a Zetasizer Nano ZSP (Malvern Instruments Ltd.). The machine was fitted with a 633 nm He-Ne laser and measurements were performed in the 173-degree backscattering mode. Measurements were done in 2 mL glass vials. The Zetasizer software output results from a cumulative fit and a distribution fit. The cumulative fit of raw data gave an average diameter and polydispersity index (PDI), and the dispersion fit gave a size distribution based on intensity, volume, or number of particles.

Credit authorship contribution statement

Cathryn G. Conner: Methodology, Data curation, Formal analysis, Investigation, Writing – original draft. **James McAndrew:** Conceptualization, Formal analysis, Funding acquisition, Writing – review & editing. **Stefano Menegatti:** Conceptualization, Writing – review & editing. **Orlin D. Velev:** Conceptualization, Methodology, Supervision, Project administration, Writing – review & editing.

Declaration of Competing Interest

The authors declare that they have no known competing financial interests or personal relationships that could have appeared to influence the work reported in this paper.

Data Availability

No data was used for the research described in the article.

Acknowledgements

This research was supported by a grant from Air Liquide, Newark DE, United States. We also acknowledge the support provided to Cathryn Conner by the NC State Molecular Biotechnology Training Program (MBTP) sponsored by the National Institutes of Health, United States and the Graduate School at North Carolina State University (5 T32 GM008776-15), and support to Orlin Velev by NSF, United States grants CMMI-1825476 and CBET-1935248. We are thankful to the Velev group members, both present and alumni, for the collaborative and encouraging work environment.

Appendix A. Supporting information

Supplementary data associated with this article can be found in the online version at doi:10.1016/j.colsurfa.2022.129833.

References

[1] P.J. Carter, Introduction to current and future protein therapeutics: a protein engineering perspective, Exp. Cell Res. 317 (9) (2011) 1261–1269, https://doi.org/10.1016/j.yexcr.2011.02.013.
[2] S. Goswami, W. Wang, T. Arakawa, S. Ohtake, Developments and challenges for MAb-based therapeutics, Antibodies 2 (3) (2013) 452–500, https://doi.org/10.3390/antib2030452.
[3] L.M. Weiner, R. Surana, S. Wang, Monoclonal antibodies: versatile platforms for cancer immunotherapy, Nat. Rev. Immunol. 10 (5) (2010) 317–327, https://doi.org/10.1038/nri2744.
[4] A. Beck, T. Wurch, C. Bailly, N. Corvaia, Strategies and challenges for the next generation of therapeutic antibodies, Nat. Rev. Immunol. 10 (5) (2010) 345–352, https://doi.org/10.1038/nri2747.
[5] R.J. Harris, S.J. Shire, C. Winter, Commercial manufacturing scale formulation and analytical characterization of therapeutic recombinant antibodies, Drug Dev. Res. 61 (3) (2004) 137–154, https://doi.org/10.1002/ddr.10344.
[6] A. Braun, L. Kwee, M.A. Labow, J. Alsenz, Protein aggregates seem to play a key role among the parameters influencing the antigenicity of Interferon Alpha (IFN-Alpha) in normal and transgenic mice, Pharm. Re. 14 (10) (1997) 1472–1478, https://doi.org/10.1023/a:1012193326789.
[7] H. Schellekens, Bioequivalence and the Immunogenicity of Biopharmaceuticals, Nat. Rev. Drug Discov. 1 (6) (2002) 457–462, https://doi.org/10.1038/nrd818.
[8] G. Invernizzi, E. Papaleo, R. Sabate, S. Ventura, Protein aggregation: mechanisms and functional consequences, Int. J. Biochem. Cell Biol. 44 (9) (2012) 1541–1554, https://doi.org/10.1016/j.biocel.2012.05.023.
[9] N. Chennamsetty, B. Helk, V. Voynov, V. Kayser, B.L. Trout, Aggregation-prone motifs in human immunoglobulin G, J. Mol. Biol. 391 (2) (2009) 404–413, https://doi.org/10.1016/j.jmb.2009.06.028.
[10] M. Berger, V. Shankar, A. Vafai, Therapeutic applications of monoclonal antibodies, Am. J. Med. Sci. 324 (1) (2002) 14–30, https://doi.org/10.1097/00000441-200207000-00004.
[11] W. Wang, C.J. Roberts, Protein aggregation – mechanisms, detection, and control, Int. J. Pharm. 550 (2018) 251–268, https://doi.org/10.1016/j.ijpharm.2018.08.043.
[12] S. Blake, S. Amin, W. Qi, M. Majumdar, E. Lewis, Colloidal stability & conformational changes in β-lactoglobulin: unfolding to self-assembly, Int. J. Mol. Sci. 16 (8) (2015) 17719–17733, https://doi.org/10.3390/ijms160817719.
[13] W. Li, P. Prabakaran, W. Chen, Z. Zhu, Y. Feng, D.S. Dimitrov, Antibody aggregation: insights from sequence and structure, Antibodies 5 (3) (2016) 19, https://doi.org/10.3390/antib5030019.
[14] H. Wu, R. Kroe-Barrett, S. Singh, A.S. Robinson, C.J. Roberts, Competing aggregation pathways for monoclonal antibodies, FEBS Lett. 588 (6) (2014) 936–941, https://doi.org/10.1016/j.febslet.2014.01.051.
[15] C.J. Roberts, Non-native protein aggregation kinetics, Biotechnol. Bioeng. 98 (5) (2007) 927–938, https://doi.org/10.1002/bit.21627.
[16] C.J. Roberts, Therapeutic protein aggregation: mechanisms, design, and control, Trends Biotechnol. 32 (7) (2014) 372–380, https://doi.org/10.1016/j.tibtech.2014.05.005.
[17] E.O. Saphire, P.W.H.I. Parren, R. Pantophlet, M.B. Zwick, G.M. Morris, P.M. Rudd, R.A. Dwek, R.L. Stanfield, D.R. Burton, I.A. Wilson, Crystal structure of a neutralizing human IgG against HIV-1: a template for vaccine design, Science 293 (5532) (2001) 1155–1159, https://doi.org/10.1126/science.1061692.
[18] S. Amani, F. Nasim, T.A. Khan, N.A. Fazili, M. Furkan, I.A. Bhat, J.M. Khan, R. H. Khan, A. Naeem, Detergent induces the formation of IgG aggregates: a multi-methodological approach, Spectrochim. Acta A. Mol. Biomol. Spectrosc. 120 (2014) 151–160, https://doi.org/10.1016/j.saa.2013.09.141.
[19] M.S. Neergaard, D.S. Kalonia, H. Parshad, A.D. Nielsen, E.H. Møller, M. van de Weert, Viscosity of high concentration protein formulations of monoclonal antibodies of the IgG1 and IgG4 subclass – prediction of viscosity through protein–protein interaction measurements, Eur. J. Pharm. Sci. 49 (3) (2013) 400–410, https://doi.org/10.1016/j.ejps.2013.04.019.
[20] L.F. Pease, J.T. Elliott, D.-H. Tsai, M.R. Zachariah, M.J. Tarlov, Determination of protein aggregation with differential mobility analysis: application to IgG antibody, Biotechnol. Bioeng. 101 (6) (2008) 1214–1222, https://doi.org/10.1002/bit.22017.
[21] J.P. Brandt, T.W. Patapoff, S.R. Aragon, Construction, MD simulation, and hydrodynamic validation of an all-atom model of a monoclonal IgG antibody, Biophys. J. 99 (3) (2010) 905–913, https://doi.org/10.1016/j.bpj.2010.05.003.
[22] Á. Szenczi, J. Kardos, G.A. Medgyesi, P. Závodszky, The effect of solvent environment on the conformation and stability of human polyclonal IgG in solution, Biologicals 34 (1) (2006) 5–14, https://doi.org/10.1016/j.biologicals.2005.06.007.
[23] A.M. Morris, M.A. Watzky, R.G. Finke, Protein aggregation kinetics, mechanism, and curve-fitting: a review of the literature, Biochim. Biophys. Acta BBA - Proteins Proteom. 2009 (3) (1794) 375–397, https://doi.org/10.1016/j.bbapap.2008.10.016.
[24] W.F. Weiss, T.M. Young, C.J. Roberts, Principles, approaches, and challenges for predicting protein aggregation rates and shelf life, J. Pharm. Sci. 98 (4) (2009) 1246–1277, https://doi.org/10.1002/jps.21521.
[25] N.R. Maddux, V. Iyer, W. Cheng, A.M.K. Youssef, S.B. Joshi, D.B. Volkin, J. P. Ralston, G. Winter, C.R. Middaugh, High throughput prediction of the long-term stability of pharmaceutical macromolecules from short-term multi-instrument spectroscopic data, J. Pharm. Sci. 103 (3) (2014) 828–839, https://doi.org/10.1002/jps.23849.
[26] J.P. Gabrielson, M.L. Brader, A.H. Pekar, K.B. Mathis, G. Winter, J.F. Carpenter, T. W. Randolph, Quantitation of aggregate levels in a recombinant humanized monoclonal antibody formulation by size-exclusion chromatography, asymmetrical flow field flow fractionation, and sedimentation velocity, J. Pharm. Sci. 96 (2) (2007) 268–279, https://doi.org/10.1002/jps.20760.
[27] H. Goetz, M. Kuschel, T. Wulff, C. Sauber, C. Miller, S. Fisher, C. Woodward, Comparison of selected analytical techniques for protein sizing, quantitation and molecular weight determination, J. Biochem. Biophys. Methods 60 (3) (2004) 281–293, https://doi.org/10.1016/j.jbbm.2004.01.007.

[28] J. Liu, J.D. Andya, S.J. Shire, A critical review of analytical ultracentrifugation and field flow fractionation methods for measuring protein aggregation, AAPS J. 8 (3) (2006) E580–E589, https://doi.org/10.1208/aapsj080367.
[29] A.P. Minton, Static light scattering from concentrated protein solutions, I: General theory for protein mixtures and application to self-associating proteins, Biophys. J. 93 (4) (2007) 1321–1328, https://doi.org/10.1529/biophysj.107.103895.
[30] C. Fernández, A.P. Minton, Static light scattering from concentrated protein solutions ii: experimental test of theory for protein mixtures and weakly self-associating proteins, Biophys. J. 96 (5) (2009) 1992–1998, https://doi.org/10.1016/j.bpj.2008.11.054.
[31] S. Yadav, T.M. Scherer, S.J. Shire, D.S. Kalonia, Use of dynamic light scattering to determine second virial coefficient in a semidilute concentration regime, Anal. Biochem. 411 (2) (2011) 292–296, https://doi.org/10.1016/j.ab.2010.12.014.
[32] M. Muschol, F. Rosenberger, Interactions in undersaturated and supersaturated lysozyme solutions: static and dynamic light scattering results, J. Chem. Phys. 103 (24) (1995) 10424–10432, https://doi.org/10.1063/1.469891.
[33] G. Thiagarajan, A. Semple, J.K. James, J.K. Cheung, M. Shameem, A comparison of biophysical characterization techniques in predicting monoclonal antibody stability, mAbs 8 (6) (2016) 1088–1097, https://doi.org/10.1080/19420862.2016.1189048.
[34] C. Lehermayr, H.-C. Mahler, K. Mäder, S. Fischer, Assessment of net charge and protein–protein interactions of different monoclonal antibodies, J. Pharm. Sci. 100 (7) (2011) 2551–2562, https://doi.org/10.1002/jps.22506.
[35] H.-J. Heidebrecht, U. Kulozik, Data concerning the fractionation of individual whey proteins and casein micelles by microfiltration with ceramic gradient membranes, Data Brief. 25 (2019), 104102, https://doi.org/10.1016/j.dib.2019.104102.
[36] R. Pecora, Dynamic light scattering measurement of nanometer particles in liquids, J. Nanopart. Res. 2 (2000) 123–131, https://doi.org/10.1023/A:1010067107182.
[37] P.A. Hassan, S. Rana, G. Verma, Making sense of brownian motion: colloid characterization by dynamic light scattering, Langmuir 31 (1) (2015) 3–12, https://doi.org/10.1021/la501789z.
[38] C. Urban, P. Schurtenberger, Characterization of turbid colloidal suspensions using light scattering techniques combined with cross-correlation methods, J. Colloid Interface Sci. 207 (1) (1998) 150–158, https://doi.org/10.1006/jcis.1998.5769.
[39] Berne, B.J. Pecora, R. Dynamic Light Scattering: With Applications to Chemistry, Biology, and Physics. Dover Publ. 2000.
[40] E.J. Yearley, P.D. Godfrin, T. Perevozchikova, H. Zhang, P. Falus, L. Porcar, M. Nagao, J.E. Curtis, P. Gawande, R. Taing, I.E. Zarraga, N.J. Wagner, Y. Liu, Observation of small cluster formation in concentrated monoclonal antibody solutions and its implications to solution viscosity, Biophys. J. 106 (8) (2014) 1763–1770, https://doi.org/10.1016/j.bpj.2014.02.036.
[41] A.P. Minton, Recent applications of light scattering measurement in the biological and biopharmaceutical sciences, Anal. Biochem. 501 (2016) 4–22, https://doi.org/10.1016/j.ab.2016.02.007.
[42] Y. Li, V. Lubchenko, P.G. Vekilov, The use of dynamic light scattering and brownian microscopy to characterize protein aggregation, Rev. Sci. Instrum. 82 (5) (2011), 053106, https://doi.org/10.1063/1.3592581.
[43] D.S. Goldberg, S.M. Bishop, A.U. Shah, H.A. Sathish, Formulation development of therapeutic monoclonal antibodies using high-throughput fluorescence and static light scattering techniques: role of conformational and colloidal stability, J. Pharm. Sci. 100 (4) (2011) 1306–1315, https://doi.org/10.1002/jps.22371.
[44] M. Doi, T. Shimada, K. Okano, Concentration fluctuation of stiff polymers. II. Dynamical structure factor of rod-like polymers in the isotropic phase, J. Chem. Phys. 88 (1988) 4070–4075, https://doi.org/10.1063/1.453861.
[45] M. Kanao, Y. Matsuda, T. Sato, Characterization of polymer solutions containing a small amount of aggregates by static and dynamic light scattering, Macromolecules 36 (2003) 2093–2102, https://doi.org/10.1021/ma0213899.
[46] A. Saluja, R.M. Fesinmeyer, S. Hogan, D.N. Brems, Y.R. Gokarn, Diffusion and sedimentation interaction parameters for measuring the second virial coefficient and their utility as predictors of protein aggregation, Biophys. J. 99 (2010) 2657–2665, https://doi.org/10.1016/j.bpj.2010.08.020.
[47] C. Zhou, W. Qi, E. Neil Lewis, J.F. Carpenter, Concomitant Raman spectroscopy and dynamic light scattering for characterization of therapeutic proteins at high concentrations, Anal. Biochem. 472 (2015) 7–20, https://doi.org/10.1016/j.ab.2014.11.016.
[48] E.N. Lewis, W. Qi, L.H. Kidder, S. Amin, S.M. Kenyon, S. Blake, Combined dynamic light scattering and raman spectroscopy approach for characterizing the aggregation of therapeutic proteins, Molecules 19 (12) (2014) 20888–20905, https://doi.org/10.3390/molecules191220888.
[49] F. Meersman, K. Heremans, Temperature-induced dissociation of protein aggregates: accessing the denatured state, Biochemistry 42 (48) (2003) 14234–14241, https://doi.org/10.1021/bi035623e.
[50] B.J. Frisken, Revisiting the method of cumulants for the analysis of dynamic light-scattering data, Appl. Opt. 40 (24) (2001) 4087–4091, https://doi.org/10.1364/AO.40.004087.
[51] K. Franks, V. Kestens, A. Braun, G. Roebben, T.P.J. Linsinger, Non-equivalence of different evaluation algorithms to derive mean particle size from dynamic light scattering data, J. Nanopart. Res. 21 (9) (2019) 195, https://doi.org/10.1007/s11051-019-4630-2.
[52] R. Ragheb, U. Nobbmann, Multiple scattering effects on intercept, size, polydispersity index, and intensity for parallel (VV) and perpendicular (VH) polarization detection in photon correlation spectroscopy, Sci. Rep. 10 (21768) (2020) 1–8, https://doi.org/10.1038/s41598-020-78872-4.
[53] J. Stetefeld, S.A. McKenna, T.R. Patel, Dynamic light scattering: a practical guide and applications in biomedical sciences, Biophys. Rev. 8 (4) (2016) 409–427, https://doi.org/10.1007/s12551-016-0218-6.
[54] R.K. Brummitt, D.P. Nesta, C.J. Roberts, Predicting accelerated aggregation rates for monoclonal antibody formulations, and challenges for low-temperature predictions, J. Pharm. Sci. 100 (10) (2011) 4234–4243, https://doi.org/10.1002/jps.22633.
[55] J. Hernández-Jiménez, A. Martínez-Ortega, A. Salmerón-García, J. Cabeza, J. C. Prados, R. Ortíz, N. Navas, Study of aggregation in therapeutic monoclonal antibodies subjected to stress and long-term stability tests by analyzing size exclusion liquid chromatographic profiles, Int. J. Biol. Macromol. 118 (2018) 511–524, https://doi.org/10.1016/j.ijbiomac.2018.06.105.
[56] A. Hawe, J.C. Kasper, W. Friess, W. Jiskoot, Structural properties of monoclonal antibody aggregates induced by freeze–thawing and thermal stress, Eur. J. Pharm. Sci. 38 (2) (2009) 79–87, https://doi.org/10.1016/j.ejps.2009.06.001.
[57] N. Martin, D. Ma, A. Herbet, D. Boquet, F.M. Winnik, C. Tribet, Prevention of thermally induced aggregation of IgG antibodies by noncovalent interaction with poly(acrylate) derivatives, Biomacromolecules 15 (8) (2014) 2952–2962, https://doi.org/10.1021/bm5005756.
[58] A.M. Tsai, J.H. van Zanten, M.J. Betenbaugh, I. Study of protein aggregation due to heat denaturation: a structural approach using circular dichroism spectroscopy, nuclear magnetic resonance, and static light scattering, Biotechnol. Bioeng. 59 (3) (1998) 273–280, https://doi.org/10.1002/(SICI)1097-0290(19980805)59:3<273::AID-BIT2>3.0.CO;2-8.
[59] H. Svilenov, U. Markoja, G. Winter, Isothermal chemical denaturation as a complementary tool to overcome limitations of thermal differential scanning fluorimetry in predicting physical stability of protein formulations, Eur. J. Pharm. Biopharm. 125 (2018) 106–113, https://doi.org/10.1016/j.ejpb.2018.01.004.
[60] V. Kayser, N. Chennamsetty, V. Voynov, B. Helk, K. Forrer, B.L. Trout, Evaluation of a non-Arrhenius model for therapeutic monoclonal antibody aggregation, J. Pharm. Sci. 100 (7) (2011) 2526–2542, https://doi.org/10.1002/jps.22493.
[61] L. Nicoud, M. Sozo, P. Arosio, A. Yates, E. Norrant, M. Morbidelli, Role of cosolutes in the aggregation kinetics of monoclonal antibodies, J. Phys. Chem. B 118 (41) (2014) 11921–11930, https://doi.org/10.1021/jp508000w.
[62] D. Kuzman, M. Bunc, M. Ravnik, F. Reiter, L. Žagar, M. Bončina, Long-term stability predictions of therapeutic monoclonal antibodies in solution using Arrhenius-based kinetics, Sci. Rep. 11 (20534) (2021) 1–15, https://doi.org/10.1038/s41598-021-99875-9.